STRUCTURAL, ELECTRIC AND MAGNETIC PROPERTIES OF (1-x)BaTiO₃+xCu_{0.1}Co_{0.9}Fe₂O₄MULTIFERROIC COMPOSITE

M. A. HAIDER¹, ISHTIAQUE M. SYED¹, A. NAHAR², FARIA FERDOUS^{1*} AND M.N.I KHAN²

¹Department of Physics, University of Dhaka, Dhaka-1000

Received on 06.02.2023, Revised received on 15.04.2023, Accepted for publication on 17.04.2023

DOI: https://doi.org/10.3329/bjphy.v30i1.79513

ABSTRACT

 $(1-x)BaTiO_3+xCu_{0.1}Co_{0.9}Fe_2O_4;(x=0.0,0.1,0.3,0.5,1.0)$ multiferroic composites were being prepared by conventional solid-state reaction process. The structure and microstructure of the prepared samples was detected by the X-ray diffractometer. The X-ray diffraction analysis confirmed the tetragonal structure for x=0.0, cubic structure for x=0.1, 0.3, 0.5 and cubic spinel structure for x=1.0. Morphological analyses were carried out by the Scanning Electron Microscope (SEM). Surface morphology confirmed that the grain size and porosity decrease with the increment of ferrite content. Magnetic properties of the prepared samples were determined by Vibrating Sample Magnetometer (VSM). The magnetic saturation (M_s) was found to increase with increasing spinel content. Dielectric constant (ε') , complex permeability (μ') , DC and AC resistivity of the composites were determined by an impedance analyzer. The dielectric constant shows dispersive behavior in the low frequency region and was frequency independent in high frequency range. Dielectric constant decreases with increasing ferrite content whereas complex permeability increases. Lower value of loss factor and higher value of relative quality factor (RQF) was obtained. Activation energy of the samples was calculated from DC resistivity which confirmed the shifting from conducting nature to semiconducting nature.

KEYWORDS: Multiferroic material, Solid-state reaction method, Magnetic and electrical properties

1. INTRODUCTION

Multiferroic materials are those materials which simultaneously demonstrate different ferroic orders like ferroelectricity, ferromagnetism, piezoelectricity etc. [1]. Recently, these materials have drawn immense advertence in research activities due to their fundamental physics and potential technological multitasking device applications [2-5]. H. Schmid first named the "multiferroic" term in 1994 [6]. In general, multiferroic materials are categorized in two groups such as single phase as well as multiferroic composites consisting of two or more than two phases. Single-phase multiferroic materials are considered to be quite exceptional in manner due to the conditions for showing ferroelectricity and ferromagnetism at the same time which is difficult to gain naturally [7-9]. Single phase multiferroic materials cannot be used in practical applications because they show weak multiferroic property which occurs in room temperature [10]. So, device based on single-phase multiferroics cannot be used in room temperature. On the other hand, multiferroic (MF) composite materials is the combination of ferroelectric and ferromagnetic materials. Hence it exhibits the magnetoelectric (ME) effect better than single-phase multiferroic materials as every phase has the independent performance at room temperature [11]. Due to its room temperature applications, MF composite becomes an excellent candidate for various application such as electronic devices, sensors, actuators, transducers etc. The ME coupling in ferromagnetic-

²Materials Science Division, Atomic Energy Centre, Dhaka-1000

^{*}Corresponding author e-mail: faria.ferdous@du.ac.bd

ferroelectric composite is observed according to the principle of "product-property" which means that noticing distinct characteristic that are missing from the individual phases [12]. These ME coupling is indirectly influenced by strain/stress in the composite [13].

Recently, Y. Shen et al. reported that by controlling the phase's molar ratio, the magnetodielectric interaction can be enhanced in the(1-x)BaTiO₃+(x)CoFe₂O₄ composite [14]. According to numerous studies, substituting different ions into the ferroelectric phase or the ferromagnetic phase can enhance the ME effect. Investigation on BaSrTiO₃/NiFe₂O₄ [15], (NiZn)Fe₂O₄-BaTiO₃ [2, 16, 17] BaTiO₃-(Ni,Cu,Zn)Fe₂O₄ [18], BaTiO₃-Ni(Co,Mn)Fe₂O₄ [19] etc. are representing the ions substitution either on the ferroelectric site or ferromagnetic site. To improve the ME features, however, no study has been done on Cu ion substitution in the ferromagnetic site. Hence, BaTiO₃ is the most studied ferroelectric material having high permittivity and low dielectric loss which can be significantly used for high speed and nonvolatile memory devices [9]. Hence, no substitution ion was added in the ferroelectric phase.

Popular methods for synthesis MF composites include vacuum-based deposition, solid-state reactions, hydrothermal, auto-combustion, sol-gel etc. [2]. Among all, conventional solid-state reaction technique is considered to be most advantageous. This method's advantages include affordability, simplicity and environmental friendliness [14].

In this research, small amount of Cu^{2+} is used in the ferromagnetic site to reduce the temperature of sintering as well as to improve the densification [20] of the MF composite. Large amount of Co^{2+} is used to improve the ferromagnetic property [21]. We represent the method of preparation of $(1-x)BaTiO_3+xCu_{0.1}Co_{0.9}Fe_2O_4$ MF composite and its various dielectric and magnetic properties are discussed.

2. EXPERIMENTAL DETAILS

2.1 Sample Preparations:

The samples were prepared by usual solid-state reaction technique using BaCO₃, TiO₂, CuO, CoO, Fe₂O₃ as raw materials. Firstly, the raw substances were taken in accordance with stoichiometric ratio. Then appropriate amount of the samples was hand-milled for 6 hours using a mortar and pestle. Then calcination of the samples was done at 600° C for 3 hours in air media. The powders were again hand-milled after calcination for 2 hours in order to make a fine mixture. Then the grounded powders were compressed into 0.3 g pellets and 1 g toroid by a hydraulic press at 10 Pa pressure. Sintering of the pelletized samples were done for 3 hours at 1200° C for BaTiO₃ (BTO) sample (x= 0) and at 1100° C for 3 hours for all other samples (x=0.1, 0.3, 0.5, 1.0) in a programmable furnace. The value of x was chosen randomly.

2.2 Characterizations:

X-ray diffraction pattern of the prepared samples were determined using Rigaku Ultima IV X-ray diffractometer which uses $CuK\alpha$ radiation of wavelength 0.1541 nm. The value of the lattice parameter of the samples was determined using the Nelson-Riley (N-R) function. The bulk density, $\rho_b = M/V$ (where M denotes the mass and V denotes the volume of the sample), theoretical density, $\rho_x = nM_1/N_A a^2$ (where n denotes the number of atom per unit cell, M_l atomic mass of the sample, N_l denotes Avogadro's Number, n is the lattice parameter) and porosity, n is n0 the samples were calculated. The surface morphology as well as microstructural analysis of the composites were done using Scanning Electron Microscope (SEM) (JSM-6490LA,

JEOL Ltd., Tokyo, Japan. The machine was operating at 20 kV field with 10000 magnifications. The magnetization of the samples was determined at room temperature by Microsense EV9 Vibrating Sample Magnetometer (VSM). Saturation magnetization (M_s) , remnant magnetization (M_r) , coercivity (H_c) and anisotropic energy have been measured from the MH hysteresis loop. Anisotropy constant was calculated using the formula: $H_c = \frac{0.98 \, \text{K}}{M_S}$. Dielectric constant (ε') , complex permeability (μ^*) and resistivity (ρ) of the samples were determined by Impedance Analyzer (WAYNE KERR 6500B). In this measurement, the tablet-shaped samples were polished carefully then silver paste was applied to both polished side of tablets to increase its conductivity. Real part of permittivity was measured by the following formula: $\varepsilon' = \frac{cd}{\varepsilon_0 A}$, where C denotes the capacitance, d denotes the thickness of the sample, ε_0 is the permittivity in vaccum and A denotes the cross sectional area of the plate and imaginary part was measured by the following formula: $\varepsilon'' = \varepsilon' t a n \delta$, where ε' is the real part of dielectric constant and $t a n \delta$ is the loss tangent or the dissipation factor. To measure complex permeability, ring-shaped samples were carefully polished. Complex permeability is defined by the following equation: $\mu^* = \mu' - i\mu''$, where μ' and μ'' denoted the real and imaginary part of the complex permeability respectively. DC resistance of the samples was determined by the Keithley (6514B) through two probe method. Current through the samples was measured by applying voltage across it in this process. The resistivity was calculated from following formula: $\rho = RA/l$; where R is resistance of the samples, A is surface area and l is the thickness of pellets. The Activation energy, E_A was calculated from the Arrhenius law from the following formula: $\rho = \rho_0 \exp\left(\frac{E_A}{K_b T}\right)$; where ρ is the resistivity at T temperature, ρ_0 is the resistivity at room temperature and K_b denotes the Boltzmann constant.

3. RESULTS AND DISCUSSION

3.1 XRD, Lattice parameters, Density and Porosity

XRD data for all samples of $(1-x)BaTiO_3+xCu_{0.1}Co_{0.9}Fe_2O_4$ MF composites are represented in fig. 1 (a-c). In Fig. 1 (a), the diffraction peaks matched well with the JCPDS card no. 05-0626 confirming that BTO phase (x=0.0) have tetragonal crystal structure [22]. The intensity of (002) peak increases with the increment of ferromagnetic phases (x=0.1, 0.3, 0.5). In Fig. 1 (b), the diffraction peak match with the JCPDS card no 221086 confirming the cubic spinel structure of $Cu_{0.1}Co_{0.9}Fe_2O_4$ phase (x=1.0) [23]. In Fig. (c), for x=0.1, the ferromagnetic peak (311) was observed at $2\theta = 35.5$ and the intensity of this peak increased for x=0.3 and 0.5. However, another ferromagnetic peak (220) was observed at $2\theta = 30$. The presence of ferromagnetic peaks in the ferroelectric phase confirmed that chemical reaction occurred between ferroelectric and ferromagnetic phases.

Table 1 represents the value of bulk and theoretical density, lattice parameter, porosity and average grain size of the samples. The mismatch between theoretical density and bulk density are because of the presence of porosity in each sample. Both bulk and theoretical density decrease with ferromagnetic phase due to the addition of the less densified ferrite content to the samples [24].

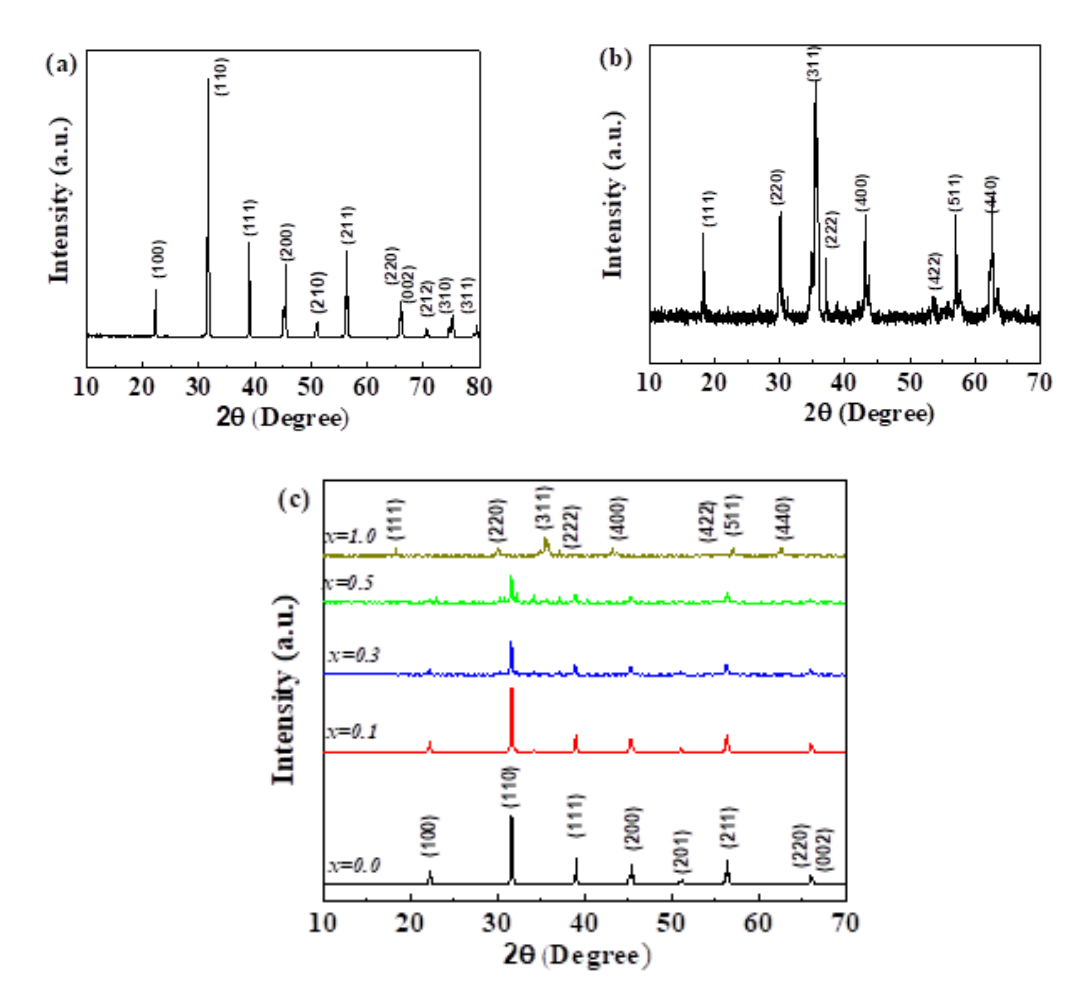


Fig.1: XRD analysis of (a) $BaTiO_3$; (b) $Cu_{0.1}Co_{0.9}Fe_2O_4$; (c) $(1-x)BaTiO_3+xCu_{0.1}Co_{0.9}Fe_2O_4$ composite; (x=0.0,0.1,0.3,0.5,1.0)

For x=1.0, the lattice parameter appears to be two times higher than in the other samples which has a strong agreement for the cubic spinel structure [23]. The value of porosity of samples reduces as the ferrite content increases. Atomic radius of Cu^{2+} (140 pm) and Co^{2+} (200 pm) are smaller than the Ba^{2+} (268 pm), when ferrite contents are added to BTO, then the vacant area may be occupied by the smaller atomic radius ions [25]. However, at x=0.3, the porosity increased to 28.32. This may be due to the stress generated by each phase of the composite.

Content,	Bulk density(g/cm ³)	Theoretical density (g/cm ³)	Lattice parameter (nm)	Porosity %	Average grain size (μm)	
x=0.0	3.985	6.036	a=b=0.3986, c= 0.40188	33.97	1.93	
x=0.1	4.300	5.990	a=b=c=0.4008	28.21	1.25	
x = 0.3	4.150	5.790	a=b=c=0.4004	28.32	1.19	
x=0.5	4.010	5.410	a=b=c=0.4001	26.43	1.11	
x=1.0	3.994	5.247	a=b=c=0.8410	23.88	1.08	

Table1: The value of bulk and theoretical density, lattice parameter and porosity for all samples.

3.2 Microstructure Analysis:

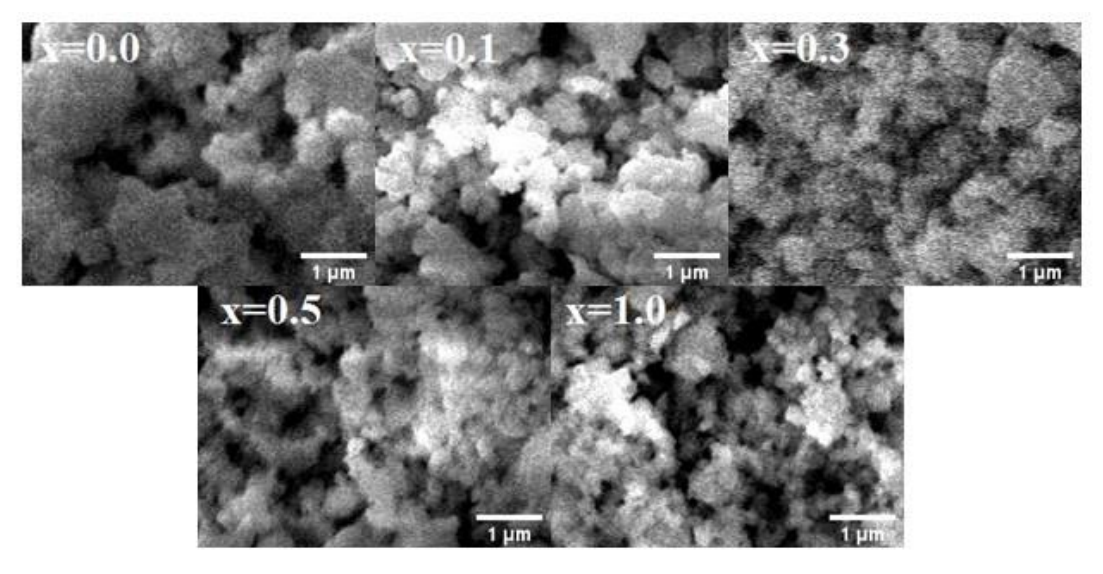


Fig. 2: FESEM images of (1-x)BaTiO₃+ xCu_{0.1}Co_{0.9}Fe₂O₄ composite (x=0.0, 0.1, 0.3, 0.5, 1.0)

Fig. 2 represents the SEM micrographs of different composites which describes microstructure and grain distribution of the samples under investigation. The microstructure of the samples depends on the substitutions used in the composite, sintering temperature and the method of synthesis. We noticed the inhomogeneity in the grain size because each phase's growth rate in composite materials is distinct. The BTO (x=0.0) have an agglomerated crystalline structure because of the higher sintering temperature. Grains and grain boundaries were appearing when the ferrite content was added. The average grain size (grain diameter) was determined from the micrographs using linear intercept method and shown in table 1. As the ferrite content rises, it has been observed that the samples' average grain size declines because a greater proportion of the ferrite content has smaller grains [25]. Additionally, the reduction in oxygen vacancies is likely to be the cause of the

grain size reduction [26]. More pores are present at grain boundaries when the grain size is reduced. As a result, the intergranular porosity reduces as shown in the XRD section [24].

3.3 M-H hysteresis loop:

Fig. 3 presents the magnetic hysteresis (M-H) curves of $(1-x)BaTiO_3+xCu_{0.1}Co_{0.9}Fe_2O_4$ MF samples. The x=0.1, 0.3, 0.5 and 1.0 samples show typical ferromagnetic behavior whereas the BTO (x=0.0) shows the non-magnetic behavior. M_s , Mr and Hc of the samples with variation of ferrite content are represented in Fig. 3(b)(c)(d), respectively. It is observed that M_s values rises as the ferrite percentage increases in the composite. In ferrite, the Fe³⁺ migrate into octahedral (B-site) while Cu²⁺ prefers to go to tetrahedral (A-site) and Co²⁺ occupies only (B-site). Fe³⁺ can therefore balance both A-sites and B-sites. As we know that if the A-B exchange interaction becomes weaker, then it will decrease the saturation magnetization based on Neel's theory ferrimagnetism [2]. The saturation magnetization fairly follows the sum rule for all the samples.

MP (composite) = (1 - x) MP (ferroelectric) + (x) MP (ferromagnetic) [10, 24]

However, sum rule is not applicable for the others magnetic parameters H_c and M_r . The H_c and M_r are correlated with the anisotropic constant. The difference between the total energy due to alignment of moment along an easy and a hard axis is known as the magnetic anisotropy energy. The anisotropy energy possesses lower value in cubic crystal due to symmetry. When the structure is tetragonal and there is at least one maximum along the path, the anisotropy energy is higher [27].

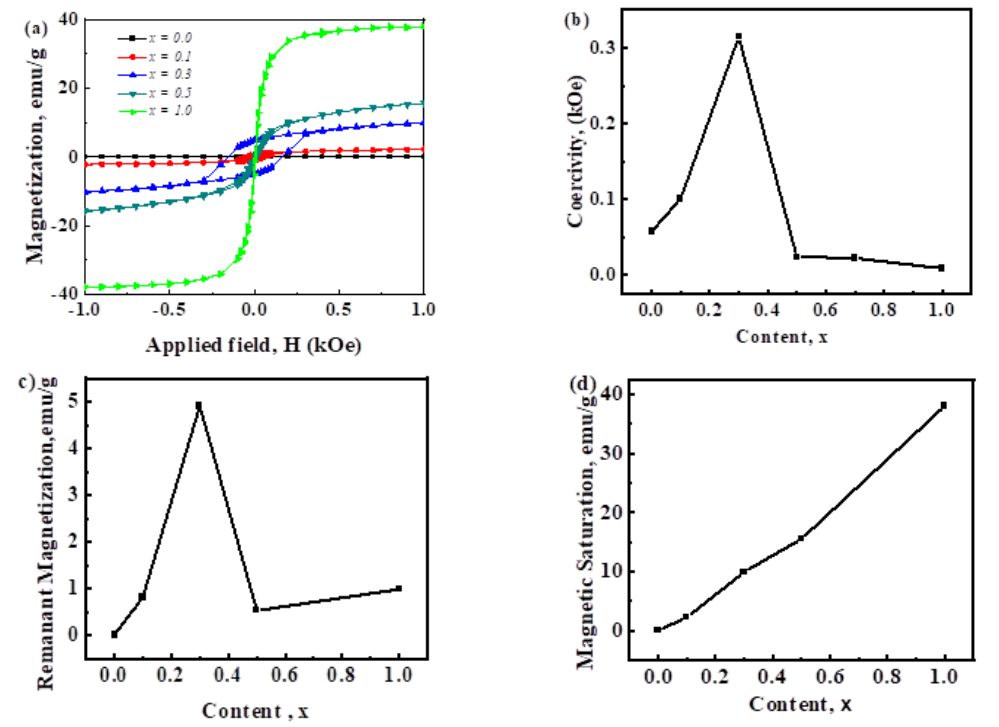


Fig. 3: (a)M-H hysteresis loop of (1-x)BaTiO₃+ xCu_{0.1}Co_{0.9}Fe₂O₄ composite (x=0.0, 0.1,0.3,0.5,1.0); (b) Coercivity; (c)Remanant Magnetization; (d) Magnetic saturation with varying ferrite content, x.

Content, x	Magnetic saturation (emu/g)	Coercivity (Oe)	Anisotropic constant (emu/cm³)	Remnant magnetization (emu/g)
0.0	0.000926	575.00	0. 2662	0.00106
0.1	2.20	1006.00	1106.0	0.8098
0.3	9.91	3144.00	155785.0	4.91
0.5	15.51	239.80	1859.0	0.524
1.0	38.01	86.35	1641.0	0.983

Table 2: The value of M_s , M_r , H_c , anisotropic energy for all samples.

3.4. Dielectric properties:

Fig. 4 (a) presents the characteristics of the real part of the dielectric constant (ε') with varying frequency (1 kHz-10000 kHz). It exhibits that the real part of the dielectric constant exhibits dispersive behavior in smaller frequency range (<10 kHz) and remains frequency independent at higher frequencies for each samples following the general behaviors of dielectric materials. At lower frequency region, all varieties of polarizations (interfacial, ionic, electronic, and dipolar) exist in the sample. With increase of frequency, interfacial and dipolar polarizations vanish slowly. So, the value of dielectric constant drops off with frequency and remains persistent at higher frequency [10]. Fig. 4 (e) shows the obtained ε' values for all samples at 1kHz at room temperature. The values of the ε' are maximum for BTO (x=0.0) and it diminishes with the rise of ferrite content and lowest value of the dielectric constant is obtained for Cu_{0.1}Co_{0.9}Fe₂O₄ (x=1). It is explainable from Maxwell-Wagner polarization of space charge in accordance with Koop's phenomenological theory [28, 29]. According to this concept, a dielectric material is consisting of conducting grains surrounded by lower conducting layer of grain boundaries. With the application of electric field, dipoles present in start moving and the charge motion in grains are intruded at grain boundaries. The results in interfacial polarization due to accumulation of the localized charge at interface. After a limiting frequency of the electric field, exchange of electron among Fe²⁺ and Fe³⁺ cannot keep pace with alternating field and the values of ε' decreases with rising frequency [30].

The loss factor of the sample with varying frequency is presented in Fig. 4(b). The dielectric loss is observed to have highest value in smaller frequency range. At higher frequency region, the loss factor reduces because of the elimination of domain wall movement. Loss factor increases with the increment of ferrite percentage in the ferroelectric material and can be understood by Debye relaxation theory. In accordance with Debye relaxation process, as the hopping frequency of electrons among various ionic sites turns nearly equal to the applied field frequency, highest dielectric loss is found [31, 32]. Composites charge carriers have reduced mobility and this causes the lower loss factor in the composites [33]. So, this can be used in microwave applications [34].

According to the Kramers-Kronig relation ($\varepsilon = \varepsilon' - i\varepsilon''$), the real and imaginary part of dielectric constant is connected. Hence if one is known, then other can be found by applying the relations [35]. Fig. 4(c) exhibits that the value of the imaginary part of the dielectric constant is smaller than the corresponding real part.

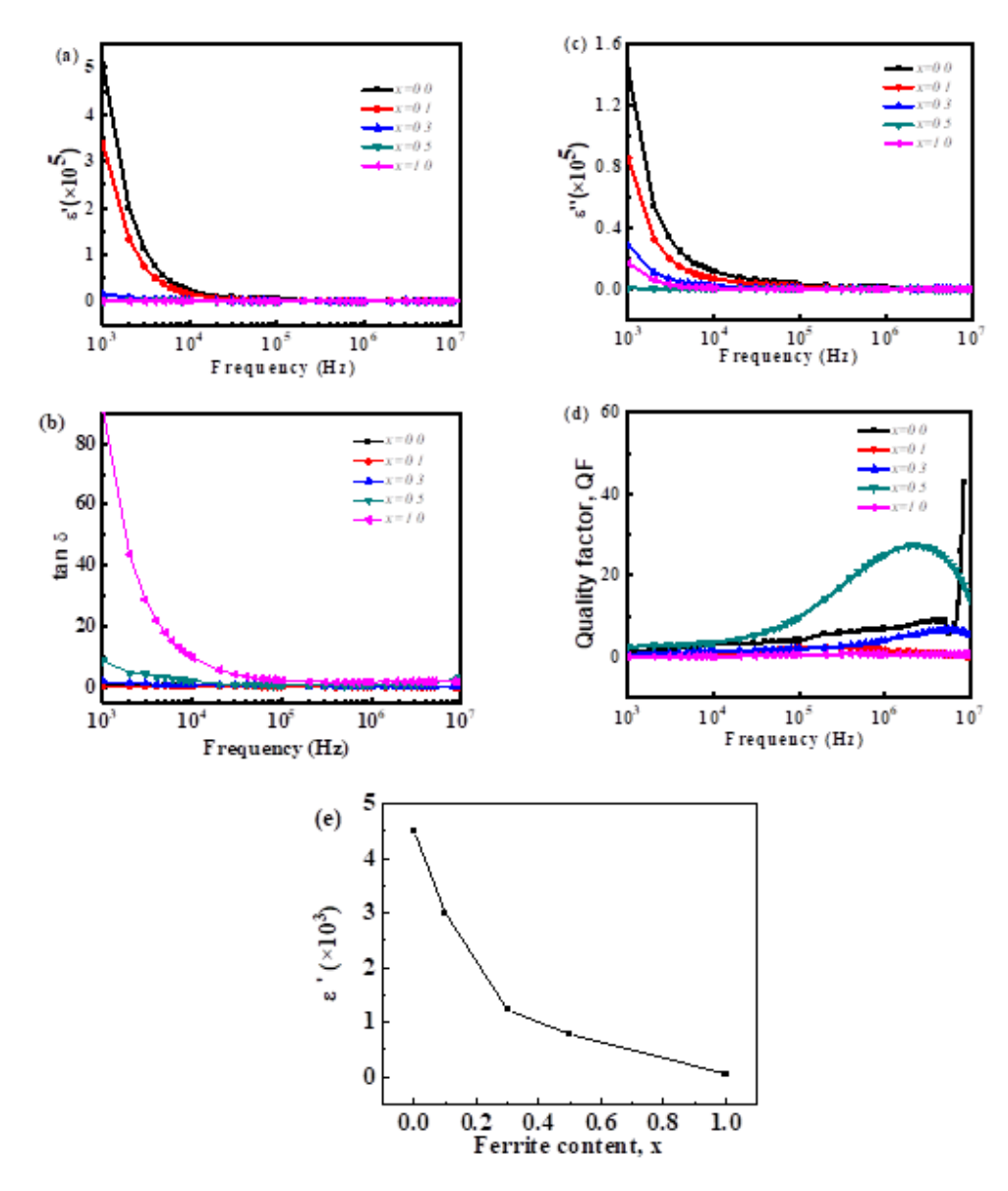


Fig. 4: (a) real part (b) loss factor (c) imaginary part (d) quality factor of dielectric constant (e) variation of real part of dielectric constant with ferrite content for $(1-x)BaTiO_3 + xCu_{0.1}Co_{0.9}Fe_2O_4$ composite as a function of frequency

3.5. Complex Permeability:

The interaction of a sample with a magnetic field can be described by its complex permeability [36]. Fig. 5 (a) shows the characteristics of the real part of the complex permeability (μ') of all

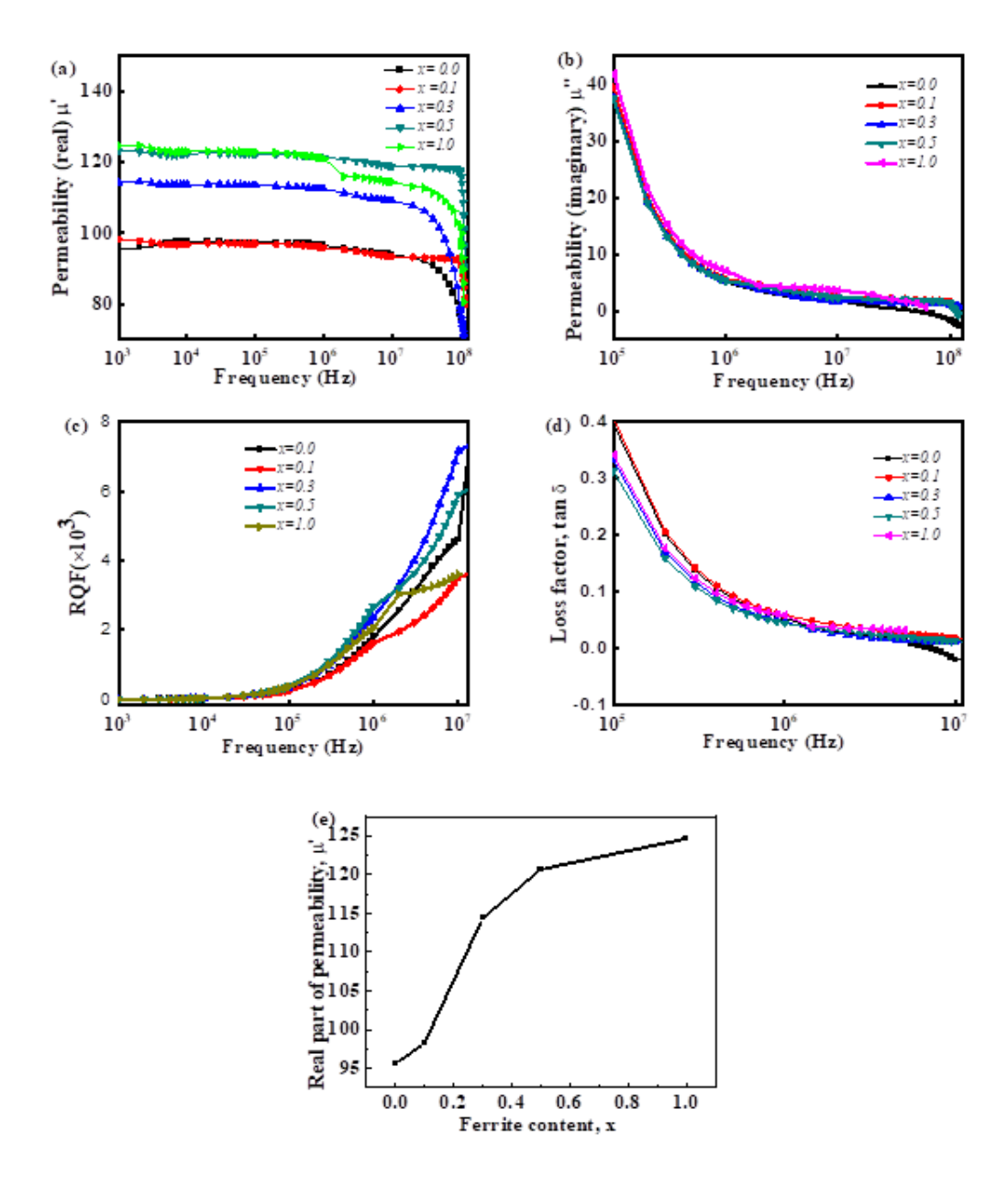


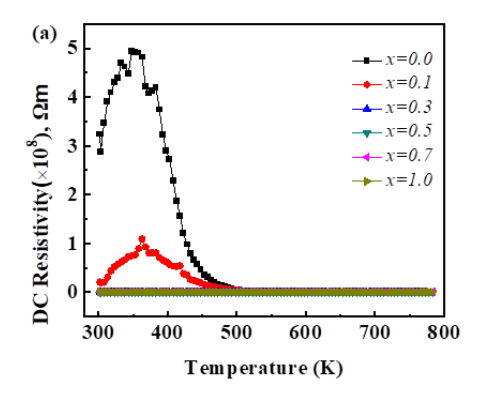
Fig. 5: Frequency dependent (a) real part of the complex permeability; (b) imaginary part of the complex permeability; (c) relative quality factor; (d) loss factor as a function of frequency (e) real part of permeability with varying ferrite content for $(1-x)BaTiO_3 + xCu_{0.1}Co_{0.9}Fe_2O_4$ composite samples (x=0.0, 0.1, 0.3, 0.5, 1.0)

samples with frequency. It was seen that μ' remains persistent until a limiting frequency level and then drops off abruptly at a certain value of frequency where its value is 71% of its initial value of permeability and it follows the Globous model [37]. When frequency is increased, the intragranular pores and impurities minimizes the spin and domain wall motion, which results in a sharp fall of μ' [24]. The frequency at which μ' starts to fall is called ferromagnetic resonance frequency (cut-off frequency) [10]. It is seen from Fig. 5(a) that the ferromagnetic resonant frequency is moved toward lower frequency range for sample x = 0.3 and 0.5 and shifted to higher frequency region for x = 0.1 and 1.0 sample. Fig. 5 (e) shows the obtained μ' values for all samples at 1kHz. The maximum value of μ' was found for sample x = 1.0 and minimum value was found for sample x = 0.0. The increase of ferrite phase increases magnetic grain interaction to enhance magnetic moment and to increase the initial permeability. Similar trend was observed in case of saturation magnetization.

Fig. 5 (b) represents change of the imaginary part of permeability (μ'') with varying frequency and it describes the dissipation of energy with varying external magnetic field. The μ'' decreases exponentially with frequency. Here the difference between the initial imaginary permeability for all samples is very small so it means dissipation energy is smaller [25]. From Fig. 5 (c) it is seen that the relative quality factor (RQF) increases with frequency. Fig. 5 (d) shows the loss factor with varying frequency and the smaller value of loss factor was found for sample x=0.5. Low loss factor and higher values of RQF is highly desirable for magnetic device applications.

3.6. DC Resistivity

DC resistivity of the samples with variation of temperature is shown in Fig. 6 (a). The DC resistivity of any composite rely on the chemical composition, hopping mechanism and sintering temperature [38]. The variation of DC electrical resistivity might be explicated by Verwey's hopping mechanism [39]. These mechanism states that, the electrical conduction in ferrites is mainly because of hopping of electrons among Fe³⁺ and Fe²⁺ ions present at B-site [39]. It is observed from Fig. 6(a) that with the increment of ferrite content in BTO, the conductivity increases so the resistivity decreases. For sample x = 0.0 and 0.1 resistivity increase until a limiting temperature and then drop off with the increase of temperature. Rise in resistivity with temperature is a conducting nature and decrease of resistivity due to mobility of hopping electron is a semiconducting nature [39]. So, for composition x = 0.0 and 0.1 sample show both conducting and semiconducting nature but other samples (x=0.3, 0.5, 1.0) show only semiconducting nature. So, the property of the samples shifted to semiconducting nature with increasing ferrite content. The Activation energy with varying ferrite content is represented in Fig. 6 (b). The energy required to remove an electron from the ion for jumping to neighboring ion, cause to happen the electrical conductivity is known as activation energy [38]. The value of activation energy for all sample are presented in table 3. Variation of activation energy in the ferroelectric phase is because of change in spin polarization and in the ferromagnetic phase it is for A-B interaction [24]. Decrease of activation energy may occur due to increasing hopping mechanism and decreasing resistivity [39].



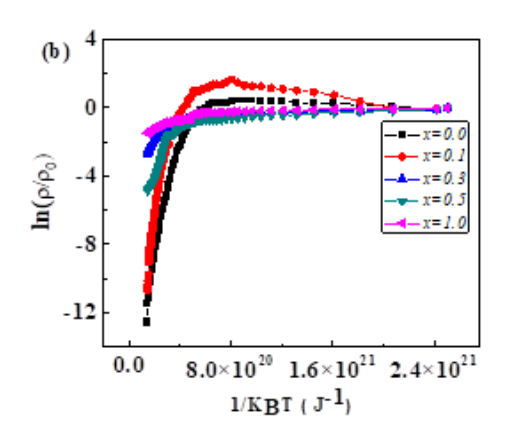
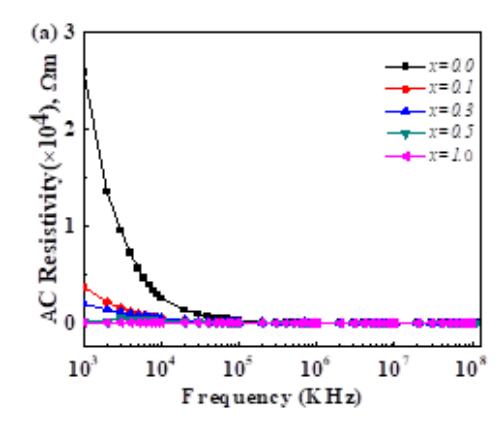


Fig. 6: (a) DC resistivity of the samples as a function of temperature; (b) graph for calculating activation energy

Table 3: Activation energy of $(1-x)BaTiO_3+xCu_{0.1}Co_{0.9}Fe_2O_4$; (x=0.0, 0.1, 0.3, 0.5, 1.0) composites.

Content	Activation Energy, EA (eV)	Activation Energy E _B (eV)
x=0.0	0.2388	0.0016
x=0.1	0.2162	0.0071
x=0.3	0.2930	0.6430
x=0.5	0.1195	0.2107
x=1.0	0.0147	0.0130

3.7. AC Resistivity



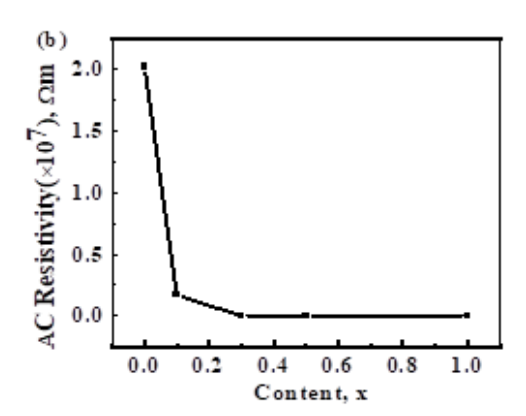


Fig. 7: (a) AC resistivity of the samples with varying frequency; (b) AC resistivity with varying ferrite content for $(1-x)BaTiO_3 + xCu_{0.1}Co_{0.9}Fe_2O_4$ composite (x=0.0, 0.1, 0.3, 0.5, 1.0).

Fig. 7 (a) represents the AC resistivity of the samples with varying frequency. Figure represents that AC resistivity diminishes with the increment of frequency. Here higher frequency increases

the hopping rate by increasing the conduction process and thus decreases resistivity [24, 40]. At higher frequency region the resistivity becomes constant because the hopping frequency cannot follow the external field [34]. Again, it has been seen from Fig. 4 (a) that dielectric constant value diminishes at a higher frequency region compelling the resistivity to decrease [41]. Fig.7(b) represents that the resistivity drops off as the ferrite content increases. The resistivity of the composite relies on composition of the materials, the grain size of the samples, grain boundaries, porosity etc. [42]. Here it was observed that BTO has larger resistivity than the ferromagnetic Cu_{0.1}Co_{0.9}Fe₂O₄. The maximum value of resistivity is found for ferroelectric phase. Since the size of grain decrease with increasing ferrite content hence the resistivity also decreases.

4. CONCLUSIONS

Multiferroic composite with chemical composition $(1-x)BaTiO_3+ xCu_{0.1}Co_{0.9}Fe_2O_4$ was successfully synthesized via standard solid state reaction process. The XRD analysis of samples confirmed tetragonal structure for x=0.0, cubic structure for x=0.1, 0.3, and 0.5 and spinel cubic structure for x=1.0 sample. The decreased porosity indicates better crystallization of all samples with the increment of ferrite content. Hence, the average size of grain was observed to decline with ferrite content. From MH hysteresis curve it can be noticed that magnetic saturation rises as the ferrite content rises and largest value of remnant magnetization was found for x=0.3 sample. Dielectric constant was found to exhibit high frequency stability and the dielectric loss was found to be very low in comparison to the dielectric constant. The largest value of dielectric Q factor was found for x=0.5. Initial value of complex permeability was observed to increases with increment of ferrite amount. The maximum value of RQF and minimum value of loss factor was obtained for x=0.5. Both AC and DC resistivity of the samples decline with increment of ferrite percentage which demonstrated the enlargement of conductive character of composites. Hence, currently investigating composites can be utilized for various multifunctional applications including spintronic device.

ACKNOWLEDGEMENTS

The authors would like to express their gratitude to the Materials Science Division, Atomic Energy Centre, Dhaka for allowing us to make greater use of the experimental facilities. During the course of this investigation, we would also like to express our appreciation to Centre for Advance Research in Science (CARS), University of Dhaka, for their cooperation as well.

Author Declarations:

The authors have no conflicts to disclose.

Data Availability Statement:

The data that support the findings of this study are available from the corresponding author upon reasonable request.

REFERENCES

[1] D.I. Khomskii, Multiferroics: Different ways to combine magnetism and ferroelectricity, Journal of Magnetism and Magnetic Materials 306 (2006) 1–8.

- [2] A. Dzunuzovic, M.M.V Petrovic, B.S Stojadinovic, N.I Ilic, J.D Bobic, C.R Foschini, M.A Zaghete, B.D. Stojanovic, Multiferroic (NiZn)Fe2O4–BaTiO3 composites prepared from nanopowders by autocombustion method, Ceramics International 41 (2015) 13189–13200.
- [3] R. Mondal, B. Murty, V. Murthy, Dielectric, magnetic and enhanced magnetoelectric response in high energy ball milling assisted BST-NZF particulate composite, Materials Chemistry and Physics 167 (2015) 338-346.
- [4] G. Srinivasan, E.T. Rasmussen, R. Hayes, Magnetoelectric effects in ferrite-lead zirconate titanate layered composites: The influence of zinc substitution in ferrites, Physical Review B. 67 (2003) 014418
- [5] Z. Yu, C. Ang, Maxwell-Wagner polarization in ceramic composites BaTiO₃-(Ni_{0.3}Zn_{0.7})Fe_{2.1}O₄, Journal of Applied Physics 91 (2002) 794 -797.
- [6] H. Schmid, Multi-ferroic magnetoelectrics, Ferroelectrics 162 (1994) 317-338.
- [7] J.V. Suchtelen, Product properties: A new application of composite materials, Philips Research Reports 27 (1972) 28-37.
- [8] N.A. Hill, Why are there so few magnetic ferroelectrics?, Journal of Physical Chemistry B 104 (2000) 6694-6709.
- [9] N. Ortega, A. Kumar, J.F. Scott, R.S. Katiyar, Multifunctional Magnetoelectric Materials for Device Applications, Journal of Physics: Condensed Matter 27 (2015) 504002.
- [10] S.C. Mazumdar, M.N.I. Khan, M.F. Islam, A.K.M. Akther Hossain, Tuning and Magnetoelectric coupling in (1-y)Bi_{0.8}Dy_{0.2}FeO₃ + yNi_{0.5}Zn_{0.5}Fe₂O₄", Journal of Magnetism and Magnetic Materials 401 (2016) 443-454.
- [11] R.M. Thankachan, R. Balakrishnan, Chapter-8 synthesis strategies of single phase and composite multiferroic nanostructures, Micro and Nano Technologies, Wood Head Publishing (2018) 185-211.
- [12] Y.D. Viehland, J.F. Li, Y. Yang, T. Costanzo, A. Yourdkhani, G. Caruntu, P. Zhou, T. Li, A. Gupta, M. Popov, G. Srinivasan, Tutorial: Product properties in multiferroic nano composites, Journal of Applied Physics 124 (2018) 061101.
- [13] Y. Wang, J. Hu, Y. Lin, C.W. Nan, Multiferroic magnetoelectric composite nanostructures, NPG Asia Materials 2 (2010) 61-68.
- [14] Y. Shen, J. Sun, L. Li, Y. Yao, C. Zhou, R. Su, Y. Yang, The enhanced magnetodielectric interaction of (1 x)BaTiO₃–xCoFeO multiferroic composites, Journal of Materials Chemistry C 2 (2014) 2545.
- [15] A. Tumarkin, N. Tyurnina, Z. Tyurnina, O. Sinelshchikova, S. Sviridov, A. Gagarin, A. Drozdovskii, E. Sapego, Composite structures BaSrTiO₃/NiFe₂O₄ for microwave applications, Ferroelectrics 592 (2022) 134-142.
- [16] L. Mitoseriu, V. Buscaglia, M. Viviani, M.T. Buscaglia, I. Pallecchi, C. Harnagea, A. Testino, V. Trefiletti, P. Nanni, A.S. Siri, BaTiO₃–(NiZn_{0.5})Fe₂O₄ ceramic composites with ferroelectric and magnetic properties, Journal of the European Ceramic Society 27 (2007) 4379-4382.
- [17] H.F. Zhang, S.W. Or, H.L.W. Chan, Fine-grained multiferroic BaTiO₃/(Ni_{0.5}Zn_{0.5})Fe₂O₄ composite ceramics synthesized by novel powder-in-sol precursor hybrid processing route, Materials Research Bulletin 44 (2009) 1339-1346.
- [18] K. Kamishima, Y. Nagashima, K. Kakizaki, N. Hiratsuka, K. Watanabe, H. Naganuma, Magnetic and Electronic Properties of BaTiO₃-(Ni,Cu,Zn)Fe₂O₄ Ceramic Composite: Reflection of Kepler Conjecture, Journal of the Physical Society of Japan 78 (2009) 124801.
- [19] V.D. Boomgaard, R.A.J. Born, A sintered magnetoelectric composite material BaTiO₃-Ni(Co,Mn) Fe₂O₄, Journal of Materials Science 13 (1978) 1538-1548.
- [20] L.B. Kong, Z.W. Li, G.Q. Lin, Y.B. Gan, Magneto dielectric properties of Mg-Cu-Co ferrite ceramics: I. densification behavior and microstructure development, Journal of the American ceramic society 90 (2007) 3106-3112.
- [21] A.L. Ortega, E. Lottini, C.D.J. Fernandez, C. Sangregorio, Exploring the magnetic effect of cobalt ferrite nano particles for the development for a rare earth free permanent magnet, Chemistry of materials 27 (2015) 4048-4056.

- [22] A. Nahar, M.A. Bhuiyan, M.J. Rahman, S. Choudhury, Enhanced Dielectric properties of Bismuth Doped Barium Titanate Ceramics with their Structural and Compositional Studies, Biointerface Research in Applied Chemistry 11 (2021) 9862-9870.
- [23] A. Nahar, K.H. Maria, S.I. Liba, M. Anwaruzzaman, M.N.I. Khan, A. Islam, S. Choudhury, S.M. Hoque, Surface-modified CoFe2O4 nanoparticles using Folate-Chitosan for cytotoxicity Studies, hyperthermia applications and Positive/Negative contrast of MRI, Journal of Magnetism and Magnetic Materials 554 (2022) 169282.
- [24] I. N. Esha, F. T. Z. Toma, M. Al-Amin, M.N.I. Khan, K.H. Maria, Synthesis of type-II based (1-x)Ba_{0.6}(Ca_{1/2}Sr_{1/2})_{0.4}Ti_{0.5}Fe_{0.5}O₃+(x)Ni_{0.40}Zn_{0.45} Cu_{0.15}Fe_{1.9}Eu_{0.1}O₄ composites via standard solid state reaction method and investigation of multiferroic properties, AIP Advances 8 (2018) 125207.
- [25] S.C. Mazumdar, M.N.I. Khan, M.F. Islam, A.K.M. Akther Hossain, Enhanced multiferroic properties in (1-y)BiFeO₃-yNi_{0.5}Cu_{0.05} Zn_{0.45}Fe₂O₄ composites, Journal of Magnetism and Magnetic Materials 390 (2015) 61-69.
- [26] K. Brinkman, T. Iijima, K. Nishida, K. Katoda, H. Funakubo, The influence of acceptor doping on the structure and electrical properties of sol-gel derived BiFeO₃ thin films, Ferroelectrics 357 (2007) 35-40.
- [27] M.S.S. Brooks, M. Richter, L.M. Sandratskii, Density Functional Theory: Magnetism, Encyclopedia of Materials: Science and Technology, Elsevier (2001) 2059-2070.
- [28] J.C. Maxwell, A treatise on electricity and magnetism, New York: Oxford University Press 1 (1998) 1-558.
- [29] K.W. Wagner, Zur theorie der unvollkommenen dielekrika", Annalen der Physik (Leipzig) 345 (1913) 817-855.
- [30] K.K. Patankar, P.D. Dombale, V.L. Mathe, S.A. Patil, R.N. Patil, AC Conductivity and magnetoelectric effect in MnFe_{1.8}Cr_{0.2}O₄ – BaTiO₃ composites, Material Science Engineering B: Advanced functional solid state-materials 87 (2001) 53-58.
- [31] H.M Abdelmoneim, Dielectric properties of Ti_x Li_{1-x}La_{0.1}Fe_{1.9}O₄ ferrite thin films, Indian Journal of Pure and Applied Physics 48 (2010) 562-570.
- [32] M.D. Rahman, S.K. Saha, T.N Ahmed, D.K Saha, A.K.M. Akther Hossain, Magnetoelectric effect of (1-x)Ba_{0.5}Sr_{0.5}Zr_{0.5}Ti_{0.5}O₃+xNi_{0.12}Mg_{0.18}Cu_{0.2}Zn_{0.5}Fe₂O₄ composites, Journal of Magnetism and Magnetic Materials 371 (2014) 112-120.
- [33] N.S Negi, A. Sharma, J. Shah, R.K. Kotnala, Investigation on impedance response, magnetic and ferroelectric properties of 0.20(Co_{1-x}Zn_xFe_{2-y}Mn_yO₄)-0.80(Pb_{0.70}Ca_{0.3}TiO₃) magnetoelectric composite, Materials chemistry and physics 148 (2014) 1221-1229.
- [34] F.T.Z Toma, I.N. Esha, M. Al-Amin, M.N.I Khan, K.H Maria, Study of the structural, electrical and magnetic properties of Ca and Sr substituted BaTiO₃ ceramics, Journal of Ceramic Processing Research 18 (2017) 701-710.
- [35] R. Lovell, Application of Kramers-Kronig relations to the interpretation of dielectric data Journal of Physics C: Solid State Physics 7 (1974) 4378.
- [36] T. Nakamura, Low-temperature sintering of Ni-Zn-Cu ferrite and its permeability spectra, Journal of magnetism and magnetic materials 168 (1997) 285-291.
- [37] A. Globus, H. Pascard, V. Cagan, Distance between magnetic ions and fundamental properties in ferrites, Journal de physique colloques 38 (1977) C1-163-C1-168.
- [38] M.K. Raju, R.R. Raju, K. Samatha, Structural, DC resistivity and activation energy of NiCuZn ferrite, Journal of optoelectronics and advanced materials 17 (2015) 1075-1079.
- [39] J.B. Goodenough, Jahn-Teller phenomena is solids, Annual Review on materials science 28 (1998) 1-27.
- [40] R. Punia, R.S. Kundu, S. Murugavel, N. Kishore, Hopping conduction in Bismuth modified Zinc vanadate glasses: An applicability of Mott's model, Journal of Applied Physics 112 (2012) 113716.
- [41] N. Hur, S. Park, P.A. Sharma, J.S. Ahn, S. Guha, S-W. Cheong, Electric polarization reversal and memory in multiferroic material induced by magnetic fields, Nature 429 (2004) 392-395.
- [42] O. Ivanov, O. Maradudina, R. Lyubushkin, Grain size effect on electrical resistivity of bulk nano grained Bi₂Te₃ material, Materials Characterization 99 (2015) 175-179.